A Robust State Estimation Method Against GNSS Outage for Unmanned Miniature Helicopters

Tak Kit Lau, Yun-hui Liu, *Fellow, IEEE* and Kai-wun Lin

Abstract—Most unmanned aerial robots use a Global Navigation Satellite System (GNSS), such as GPS, GLONASS, and Galileo, for their navigation. However, from time to time the GNSS fails to function due to geographical restrictions and deliberated jamming. This paper proposes an Unscented Kalman Filter-based GPS/IMU integration method in order to accurately estimate the position and velocity of an unmanned miniature helicopter even when the GNSS malfunctions completely. Different from previous GPS/IMU integration methods that cannot propagate noisy inertial measurements to the position and velocity estimations on the rapid vibratory Vertical Take-Off and Landing (VTOL) platforms during the GNSS outage, this method novelly prioritises the propagations of the states in the Unscented Kalman Filter (UKF) algorithm and leverages the time-varying GNSS dilution of precision in line with the adjustments of the measurement noise covariances. Moreover, this method models the stochastic process in the inertial sensors by the acceleration white noise bias in addition to the commonly used random walking process. Without considering the specific actuation models that vary from vehicle to vehicle, this method can particularly be applied to the quivering unmanned helicopters which equipped with two-stroke engines. It yields a rapid and precise compensation for the sensor errors in order to effectively facilitate the propagations of inertial measurements to the position and velocity estimations. Finally, the superior performance of the proposed method in terms of accuracy and endurance is empirically demonstrated using our fully instrumented JR Voyager GSR helicopter.

I. INTRODUCTION

Blossoming UAV progressions lead to the development of the anti-UAV technology. One of the greatest challenges to UAV deployments is the GNSS outage problem [1]. Let alone the spoofing attack, scenarios like deliberate jamming [2], weak satellite signal and multipathing can bring down autonomous aerial agents which solely rely on the vulnerable GNSS to georeference themselves [3][4]. While visual odometer [5] and SLAM [6] depend largely on visibility, and the anti-jamming GPS technology can only suppress interference [7][8], the inertial measurement unit's jam-free and all-weather nature provide a more promising reference to aid the GNSS among all other sensors. However, the vigorously vibrating engine, particularly on the VTOL vehicles, deteriorates the readings from the vibration-sensitive Inertial Measurement Unit (IMU), and therefore it is more challenging for the autonomous gasoline helicopters to salvage useful information from the noisy inertial measurements in order to deduce the position and velocity. Among various types of state estimation methods including the particle filter, complementary filter and recursive Bayesian estimation, the

Fig. 1: The fully instrumented JR Voyager GSR260 for experiments. The IMU is mounted on wire-rope isolators to avoid saturations.

family of Kalman filters are often applied in virtue of its reasonable processing complexity and its extensive framework to incorporate with multiple sensors. For the state estimation using the family of Kalman filters, some patents [9][10] describe GPS/INS integrated state estimation solutions for aerial vehicles. The method by Abbott [9] differs from the method by van der Merwe [10] in the consideration of the code delay error and the Doppler frequency error. Abbott linearised the nonlinear measurement models in order to cooperate with the extended Kalman filter. On the other hand, the method by van der Merwe [10] did not consider errors due to the ionosphere and Doppler effects explicitly. Instead, it modeled the sensor errors and augmented the states when using the Sigma-Point Kalman filter (SPKF) which is the root of the UKF. For this reason, the process and measurement models are not linearised. And hence the nonlinearities in the state estimation filter are preserved. The method by Abbott [9] was analysed in [11] by a simulation utilising the filter with a precision guided munition (PGM) and the method by van der Merwe [10] was experimentally analysed and demonstrated on an instrumented helicopter in [12]. Other related work [13] attempted to integrate KF-based GPS/IMU method for the unmanned quad-rotor aerial robot but failed to maintain a reasonable accuracy when GPS malfunctions. A potential solution is to design a cost function [14], which is formed by the errors of the innovations and estimations, and hence the noise covariances can accordingly adapt to the varying influences by the measurement noises, but it still cannot deal with the case when certain measuring units are totally lost. As a whole, although the aforesaid methods, which are based on Extended Kalman Filter (EKF) and UKF, successfully demonstrated to fuse measurements from multiple sensors and to obtain reliable state estimations for UAVs in flight using different designs of process and measurement models, they all cannot address the divergence and underestimation problem when the GNSS experiences a blackout.

Other than the attempts to integrate GPS and IMU for the state estimation on UAV, other methods including visual odometers and SLAM were also studied over the years. In addition to the aforesaid methods, the Defense Advanced Research Projects Agency (DARPA) is working on a project named Robust Surface Navigation (RSN) [15] which aims at

developing a solution that can position in GPS-denial area with aids from RF-transmitting beacons. As a whole, except the obvious drawback of being sensitive to vibrations, using inertial sensors to aid GNSS is more promising than using the vision or third party referencing beacons because of the jam-proof and all-weather nature of the inertial sensors.

Based on the method by van der Merwe [10] which is the first patent and publication which successfully demonstrated the use of the UKF in the GPS/IMU integrated navigation on the helicopters, this paper extends their work to deal with the state estimation under the GNSS outage by prioritising the propagation of states in the measurement-update steps of the UKF algorithm, and leveraging the GNSS dilution of precision in line with the adjustments of measurement noise covariances. Moreover, this method models the stochastic process of the inertial sensors not only by the commonly used random walks but also by the acceleration white noise bias. And hence during the GNSS blackout, the previous method [10] can be empowered to salvage and propagate the useful information in the corrupted acceleration measurements to the position and velocity estimations without encountering the issues of underestimation and divergence of the estimation errors.

II. Sensor Noises

For a GPS/IMU integrated navigation system, the only available sensor for navigation is the IMU when the GPS fails to work. In general, an IMU is composed of rate gyros, thermometers, accelerometers, and sometimes magnetometers. It outputs attitude and acceleration information. The attitude measurement, in forms of Euler angles or quaternions, is often drift-free due to the constant calibrations by the measurements of magnetic fields, temperature and the direction of gravity [16]. And hence the attitude measurement is reliable even after a long operation. The acceleration output, however, is more vulnerable to vibrations. To formulate a method to deduce the position and velocity from the outputs by the IMU, it is crucial to identify the major source that influences the resultant accuracy most. In this section, we determine this influential source on the error equation of the position estimation by the sensitivity analysis.

A. Sensitivity Analysis of Estimation Accuracy

To increase the accuracy of the state estimation, a straight-forward method is to compensate for the sensor errors by modeling them [17][18][19]. Generally there are two sources of errors in the estimation of the position and velocity: Attitude errors and measurement errors of the accelerations.

The attitude errors are composed of the fixed bias, acceleration-dependent bias, aniso-elastic bias, aniso-inertia errors, scale-factor errors, cross-coupling errors and angular acceleration sensitivity [20]. To express the error of the position estimation, it is important to look into the kind of IMU in our study. Today, thanks to the advancement of MEMS technology, the mechanical inertial sensors that involve a spinning gyroscope or a swinging pendulum are replaced by the strapdown inertial units. The mechanism of strapdown inertial device is widely investigated and documented over the last decade [17][21]. The IMU which is implemented in this method is of strapdown measurement units as well. The IMU model in this study is Xsens MTi. It exhibits less than $0.5\,^{\circ}$ and $1\,^{\circ}$ of static accuracies in roll/pitch and heading, and its root-mean-square dynamic accuracy in attitude is $2\,^{\circ}$ with a $0.05\,^{\circ}$ angular resolution under 1σ standard deviation of zero-mean angular random walk. The IMU, as shown in Fig. 10, is situated on four wire rope isolators (CR1-400S) from ITT Enidine Inc. to avoid saturations. To write the
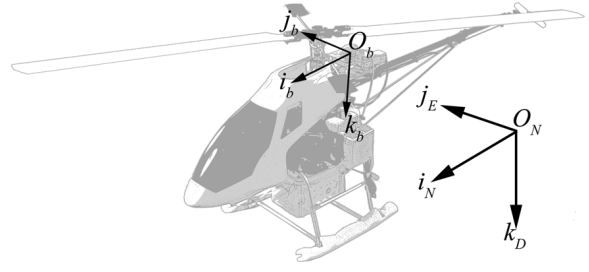

Fig. 2: The navigation frame is defined in the North-East-Downwards convention, and the body frame is at the sensor frame of the IMU.

error equation of the position, the coordinate frames are first defined.

For the convenience of the flight navigation, except the inertial frame and the body frame on the helicopter, the navigation frame is also the frame of reference. The body frame is located at the sensor frame of the IMU, and therefore the hammering acceleration can be avoided. The coordinate frames are shown in Fig. 2. The rate of velocity of the helicopter with respect to the navigation frame can be derived as,

$$\dot{\mathbf{v}}_n = \mathbf{C}_b^n \bar{\mathbf{a}}_b + \left(2\boldsymbol{\omega}_e^I + \boldsymbol{\omega}_n^e\right) \times \mathbf{v} + \mathbf{g}_l \tag{1}$$

where $\mathbf{C}_b^n$ is the transformation matrix from the body frame to the navigation frame. $\bar{\mathbf{a}}_b$ is noise-free body acceleration measurement by the IMU, hence it is with respect to the body frame. $\boldsymbol{\omega}_e^I$ is the Earth rate with respect to the inertial frame. $\boldsymbol{\omega}_n^e$ is the turn rate of the navigation frame with respect to the Earth. In the rest of the paper, $\bar{\cdot}$ refers to the noise-free measurement, $\hat{\cdot}$ refers to the estimation, $\tilde{\cdot}$ refers to the noisy measurement. Consider,

$$\Delta\mathbf{p_n} = \int_0^T \Delta\dot{\mathbf{v}}_n \, dt \tag{2}$$

where $\Delta\mathbf{p_n}$ is the position error, such that $\Delta\mathbf{p_n} = \hat{\mathbf{p}}_n - \mathbf{p}_n$, $\mathbf{p}_n$ is the position of the vehicle with respect to the navigation frame and is expressed in the navigation frame. $\hat{\mathbf{p}}_n$ is the position estimation. $\Delta\mathbf{v}_n$ is the velocity error. T is the total time length. $\mathbf{g}_l$ is the local gravity, such that $\mathbf{g}_l = \mathbf{g} - \boldsymbol{\omega}_e^I \times \left(\boldsymbol{\omega}_e^I \times \mathbf{R}\right)$. $\mathbf{R}$ is the position of the origin of navigation frame with respect to the origin of Earth frame. The estimated rate of the velocity can then be written in the same form as in (1). Differencing the two velocities for the estimation error,

$$\Delta\dot{\mathbf{v}}_\mathbf{n} = \dot{\hat{\mathbf{v}}}_\mathbf{n} - \dot{\mathbf{v}}_\mathbf{n} \tag{3}$$

$$= \hat{\mathbf{C}}_b^n \hat{\mathbf{a}}_\mathbf{b} - \mathbf{C}_b^n \mathbf{a}_b + \left(2\hat{\boldsymbol{\omega}}_e^I + \hat{\boldsymbol{\omega}}_n^e\right) \times \hat{\mathbf{v}} - \left(2\boldsymbol{\omega}_e^I + \boldsymbol{\omega}_n^e\right) \times \mathbf{v} + \Delta\mathbf{g}$$

$$= (\mathbf{I} + \boldsymbol{\Gamma}) \, \mathbf{C_b^n} \left(\Delta\mathbf{a_b} + \mathbf{a_b}\right) - \mathbf{C_b^n} \mathbf{a_b} - \left(2\boldsymbol{\omega}_\mathbf{e}^\mathbf{I} + \boldsymbol{\omega}_\mathbf{n}^\mathbf{e}\right) \times \mathbf{v} + \Delta\mathbf{g}$$

$$+ \left[2\left(\Delta\omega_\mathbf{e}^\mathbf{I} + \omega_\mathbf{e}^\mathbf{I}\right) + \left(\Delta\omega_\mathbf{n}^\mathbf{e} + \omega_\mathbf{n}^\mathbf{e}\right)\right] \times (\Delta\mathbf{v} + \mathbf{v}) \tag{4}$$

where $\mathbf{C}_b^I$ is the transformation matrix from the body frame to the inertial frame. $\Delta\mathbf{g}$ is the gravity error. $\boldsymbol{\Gamma}$ is the skew symmetric matrix of the attitude error $\begin{bmatrix} \Delta\phi & \Delta\theta & \Delta\psi \end{bmatrix}^T$ for roll, pitch and yaw. Assuming that the error of gravity estimation is small, Coriolis effect is insignificant, the product of error terms are small and the states are static. The sensitivity analyses can be performed on (3) and the influence of the attitude and acceleration measurement errors to the position estimation errors can be analyzed.

The analyses are performed by using the Monte Carlo method instead of Jacobian, which is a method of obtaining the first order partial derivatives on the outputs with respect to each input parameter, because the method of using Jacobian fails to take the statistical distribution of each

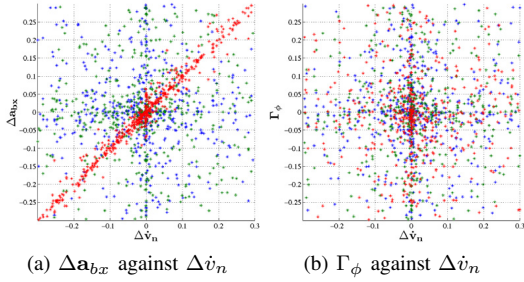(a) $\Delta\mathbf{a}_{bx}$ against $\Delta\dot{v}_n$ (b) Γ_ϕ against $\Delta\dot{v}_n$

Fig. 3: Analysis results using the Monte Carlo method. The resultant diagonal line in (a) indicates a strong correlation between the accuracy of the position estimation and the measured acceleration by the accelerometers when comparing to (b). Similar results are obtained in other channels and hence are not shown.

item in the analytical form into account [22]. Assume that both input parameters, the attitude error and the acceleration measurement error, are of zero-mean white noises, such that,

$$\Delta\mathbf{a}_b \sim \mathcal{N}(0, \boldsymbol{\sigma}_{\Delta\mathbf{a}_b}) \text{ and } \boldsymbol{\Gamma} \sim \mathcal{N}(0, \boldsymbol{\sigma}_\Gamma)$$

where $\boldsymbol{\sigma}_{\Delta\mathbf{a}_b}$ and $\boldsymbol{\sigma}_\Gamma$ are the variances of the acceleration error and the attitude error. From Fig. 3, it is observed that the outputs of the analytical form in (3) demonstrate a strong correlation with the acceleration error compared to the attitude error. This result indicates that the accuracy of the position estimation is susceptible to the acceleration measurement errors, and the attitude error influences relatively less to the position estimations as long as the following relation is satisfied,

$$\mathbf{R}_x(\Delta\phi)\mathbf{R}_y(\Delta\theta)\mathbf{R}_z(\Delta\psi) \approx \mathbf{I} + \boldsymbol{\Gamma} \tag{5}$$

From the Monte Carlo method, the accuracy of the position estimation depends largely on the acceleration measurement errors, so it is reasonable to expect a significant improvement on the position estimations when the accuracy of the acceleration measurements are improved. Based on this analysis, the sources of errors in the acceleration measurements are further investigated in order to achieve an effective noise compensation.

B. Sensor Error Characteristics

As described in the previous sections, the acceleration measurement errors are a gala of a wide range of error items [17][23], and are subjected to the vibration, sensor assembly and fabrication procedures. And these sources of errors eventually reflect to the quantization error, velocity/position random walk, bias instability, rate random walk and drift rate ramp [17][20]. Although the present accelerometers often have immunity to the vibro-pendulous error, the variations on the noise coefficients, even identified, require constant re-calibrations from time to time. Otherwise, these variations severely deteriorate the estimation accuracy in the progress of time.

Identification of the noise characteristics can help us to precisely model and design an algorithm for the state estimation. In the previous sections, it is found that the measurement errors of the accelerations play a major role in the position estimation errors. Different from previous works that categorized the errors into different items and identified them in a piecewise manner, this study aims at capturing the prime factor that governs the measurement errors so as to pin-point this prime noise factor and to maximize and eventually improve the accuracies of the position and velocity estimations.

The acceleration measurement is analysed by the Allan variance [24] in view of its avail in both time and frequency

domains. The Allan variance can be evaluated by using this formula,

$$\sigma_A^2(\tau) = \frac{1}{2\tau^2(N-2m)} \sum_{k=1}^{N-2m} (a_{k+2m} - 2a_{k+m} + a_k)^2 \tag{6}$$

where σ_A is the Allan variance. τ is the time length. N is the total number of samples. m forms the current τ with the initial time length, such that $\tau = m\tau_o$. a_k is the kth acceleration measurement.

The data in this analysis are measured by the Xsens MTi which is an IMU equipped on our fully instrumented two-stroke engine miniature helicopter. Fig. 4 shows the variation of the Allan variance in the progress of time length in a bin for differencing. The plot indicates that the variance decreases gradually as the time length increases, and reaches a minimum point between 10^0 and 10^1 seconds before reviving up. The noise items, including the quantization error due to the finite bit resolution in the analog-to-digital converters during digitization, velocity random walk, correlated noise, bias instability, rate random walk and rate ramp, are identified using the slopes and line shapes [25]. From the analysis by Allan variance, we not only find that the acceleration measurement is rich of various types of noises that characterise differently in a function of the time length. It is also observed that although the measurement unit is of a strapdown inertial unit, its calibrated acceleration readings are still significantly haunted by the stochastic processes. Different from the prior work that further decomposed the results obtained by the Allan variance and span into numerous dimensions for the sensor noise compensation, this study takes another perspective by considering that all forms of noise items are additive. Since the purpose is not to obtain an accurate acceleration output but the position and velocity estimations, this study does not pin-point each noise coefficient, instead it further analyses the outcomes that these noise coefficients eventually reflect to. And these outcomes are the position and velocity estimations.

C. Random Walk Acceleration Noise

Fig. 5 (a) and Fig. 6 (a) show the velocity and position estimations obtained from the inertial measurement unit through the time-step integrations for ten series of data. The acceleration measurements are collected statically from the inertial measurement unit at 100Hz. The velocity estimation diverges linearly, while the position estimation diverges exponentially as expected,

$$\delta\mathbf{p} = \tilde{\mathbf{p}} - \bar{\mathbf{p}} = \int_0^T \left(\int_0^T \bar{\mathbf{a}} + \sum \boldsymbol{\varepsilon}_\mathbf{a} \, dt \right) dt - \bar{\mathbf{p}} \propto T^2 \tag{7}$$

where $\delta\mathbf{p}$ is the measurement noise in the position, $\tilde{\mathbf{p}}$ is the noisy acceleration measurement, $\bar{\mathbf{p}}$ and $\bar{\mathbf{a}}$ are the noise-free position and acceleration measurements, $\sum \boldsymbol{\varepsilon}_a$ is the sum of all noise terms in the acceleration measurements.

In Fig. 5 (b,c) and Fig. 6 (b,c), these figures exhibit the velocity and position estimations by the accelerations which are simulated by the random walk and the white noise random process. It is observable that the actual patterns of divergence differ from the ones generated by the accelerations which are modeled as random processes. Therefore, without decomposing the sum of all noise terms in (7), this study models the influence of the stochastic process on the velocity and position estimation by its accumulating attribute, i.e. the random walk process, after comparing the divergence patterns in Fig. 5 and 6. That is,

$$\dot{\mathbf{a}}_b = \mathbf{w}_{a_b} \tag{8}$$

$$\mathbf{w}_{a_b} \sim \mathcal{N}\left(0, \boldsymbol{\sigma}_{\mathbf{w}_{a_b}}\right) \tag{9}$$
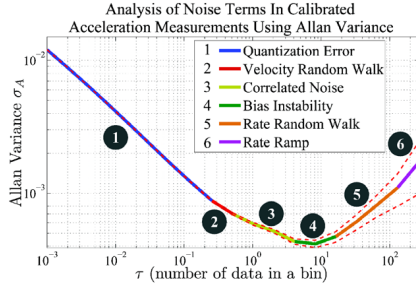
Fig. 4: This figure shows the variation of Allan variances against the progress of time length for a series of acceleration measurement by the inertial measurement unit. Each segment is categorized into different types of noise terms [25]. The dotted lines indicate the error boundary [24], such that $\varepsilon_{\sigma_A} = \sqrt{2(N/\tau - 1)}^{-1}$. This plot remains valid for up to 20 minutes of characteristic time. Only the x-axis of the body frame is shown.
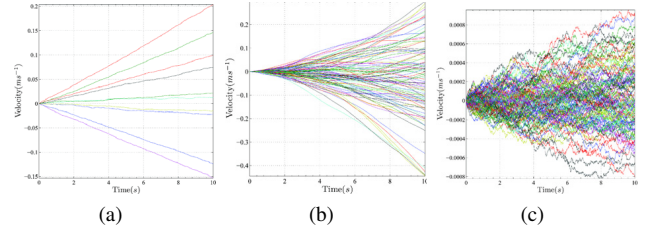

Fig. 5: These figures plot the velocity estimations deduced from three kinds of acceleration. (a) From calibrated accelerations measured statically by Xsens MTi IMU at 100Hz. (b) From accelerations simulated by the random walk process. (c) From accelerations simulated by the random white noise process.
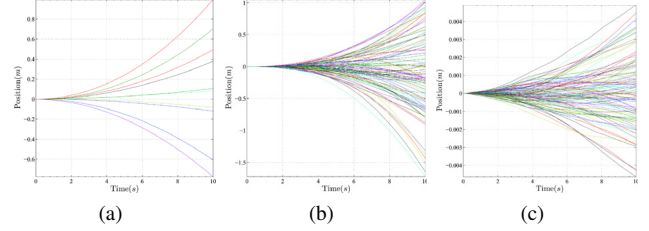

Fig. 6: Integrating the velocity estimation in Fig. 5, the position estimations are obtained accordingly.

In fact the simple but effective form of the random walk process is widely applied in the modeling of inertial sensors [19][18][20]. However, different from previous work [10][12] that model the noises in the acceleration measurement by the random walk and several constant coefficients. This study proposes to model the acceleration measurement with an extra term called the acceleration white noise bias (AWNB). That is,

$$\bar{\mathbf{a}} = \tilde{\mathbf{a}} - \mathbf{a}_b - \mathbf{n}_b - \mathbf{a}_w \quad (10)$$

$$\dot{\mathbf{a}}_w = 0 \quad (11)$$

where $\mathbf{a}_w$ is the acceleration white noise bias, and $\mathbf{n}_b$ is a constant noise term. AWNB is modeled as the states in the UKF hence they vary and converge although its rate of change is modeled as zeros. From the perspective of the effective error minimization, the proposed extra term in the modeling of the sensor error is in analogue to a dual-gear calibration system as shown in Fig. 7. The position of the pointer (top yellow triangle) can be more effectively adjusted than a single-gear design. Similarly, adding a to-be-predicted constant bias as a noise term can estimate the acceleration effectively because the sooner the drifting noise is compensated, the more accurate estimation can be achieved. Therefore, putting the AWNB in the equation along with the original random-walking noise terms can speed up the changing rate of the estimated value, and hence the drifting noises can be compensated at an earlier stage. As a result, the overall performance is improved. This claim is confirmed in the experiments (Section IV). In addition, in another attempt the AWNB is transformed and acts as an acceleration scale (AS) to the noisy acceleration measurement but the result is not satisfactory as being an additive term. The comparison is shown in Table I as well.

III. STATE ESTIMATION ALGORITHM

The structure of the proposed state estimation algorithm is illustrated in Fig. 8. The outline of the main idea is that the acceleration measurements influentially determine the position and velocity estimation errors and hence they must be compensated effectively before the propagations. It is found that the commonly used random walking process is not sufficient to model the stochastic process of the acceleration measurements by the IMU. As a result this study proposes to add the acceleration white noise biases to the modeling of the sensor error equations in order to achieve a rapid and precise sensor error compensation. On the other hand, from the original UKF framework, each state are propagated from its related ancestors obtained in the previous iteration to the
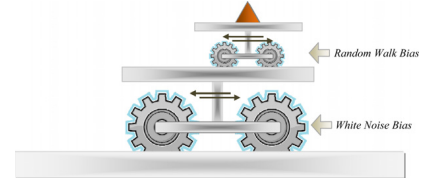

Fig. 7: A dual gear mechanism which is an analogue of having both the random walking bias and the proposed white noise bias for the sensor noise compensation. In this mechanism, the lower gears can position the upper gears for further fine-tuning process on the top-most triangle pointer.
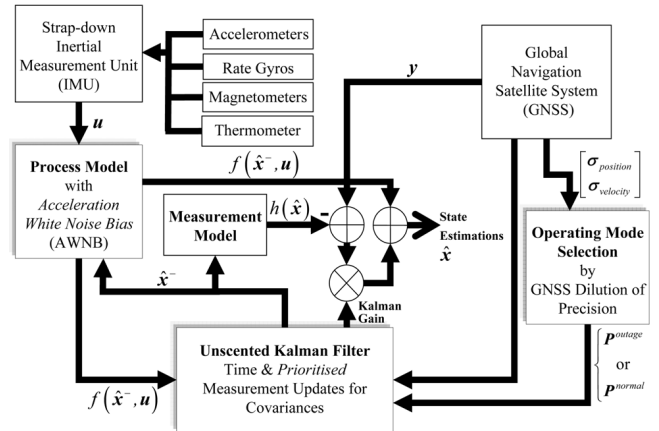

Fig. 8: The structure of the proposed state estimation algorithm.

next hierarchy of state. And hence the position estimations are delayed and undervalued especially when the GNSS malfunctions. Therefore the proposed method prioritises the measurement-update steps in the original UKF algorithm so that the states of the position can inherit the latest velocity and acceleration estimations in each iteration. Lastly, during the GNSS outage, more emphases should be allocated to the inertial measurements. Therefore, this method proposes to augment the measurement noise covariances between the GNSS and IMU readings according to the time-varying GNSS dilution of precision. And hence the state estimation can adapt to the correct operating mode without underestimating or overrating the measurement inputs.

A. Process and Measurement Models

For the sensor error modeling of the acceleration measurements, based on the analysis that the acceleration measurement errors influences the position estimations most, this study focuses on compensating the noise items in the acceleration measurements and propose to model the sensor error with the acceleration white noise bias along with the commonly used random walk process. As shown in Eq. (11) the random walk bias and the acceleration white noise bias have to be updated to the optimal values for an accurate error compensation. Without using the particle filter [26] which makes no assumption on the stochastic process underneath and hence computationally expensive, this study utilises one of the variants of the sigma-point Kalman filter [27], the UKF, in order to obtain the optimal estimation of noise terms shown in Eq. (11) for the compensation of the sensor errors. UKF implements the sigma points which are generated by considering the variance of each state and are applied to the exact nonlinear process and measurement models without losing generality. Also, in each iteration, the sigma-points are weighted to formulate a sum to yield an estimate that captures all variations in the process. For the process and measurement models inside the filter, this study furthers the sensor and process model in [12] and extend them to deal with the state estimation on the vibratory helicopter platforms when the GPS malfunctions completely. Before detailing the enhancement on the original UKF algorithm to deal with state estimation on the vibratory helicopter platforms using the IMU only when GPS fails, the whole modified sensor and process models which evolved from [12] are first presented.

Consider that the Earth rate and the angular velocity of the helicopter are insignificant, so rewriting (1),

$$\dot{\mathbf{v}}_n = \mathbf{C}_b^n \bar{\mathbf{a}} + \mathbf{g} \tag{12}$$

Recall the proposed sensor error models in section II-C. Substituting (10) into (12) leads to,

$$\dot{\mathbf{v}}_n = \mathbf{C}_b^n \left(\tilde{\mathbf{a}} - \mathbf{a}_b - \mathbf{n}_b - \mathbf{a}_w \right) + \mathbf{g} \tag{13}$$

For the transformation matrix from the body frame to the navigation frame, the quaternion is ultilised instead of Euler angles in virtue of not involving computationally demanding trigonometrical functions. The typical quaternion representation and its rate [28] are as follows,

$$\mathbf{C}_b^I = 2 \begin{bmatrix} 0.5 - e_2^2 - e_3^2 & e_1 e_2 - e_0 e_3 & e_1 e_3 + e_0 e_2 \\ e_1 e_2 + e_0 e_3 & 0.5 - e_1^2 - e_3^2 & e_2 e_3 - e_0 e_1 \\ e_1 e_3 - e_0 e_2 & e_2 e_3 + e_0 e_1 & 0.5 - e_1^2 - e_2^2 \end{bmatrix} \tag{14}$$

$$\dot{\mathbf{q}} = \frac{1}{2} \boldsymbol{\omega}_q \mathbf{q} \tag{15}$$

where,

$$\mathbf{q} = \begin{bmatrix} e_0 & e_1 & e_2 & e_3 \end{bmatrix}^T$$

$$\boldsymbol{\omega}_q = \begin{bmatrix} 0 & \bar{\omega}_p & \bar{\omega}_q & \bar{\omega}_r \\ -\bar{\omega}_p & 0 & -\bar{\omega}_r & \bar{\omega}_q \\ -\bar{\omega}_q & \bar{\omega}_r & 0 & -\bar{\omega}_p \\ -\bar{\omega}_r & -\bar{\omega}_q & \bar{\omega}_p & 0 \end{bmatrix} \tag{16}$$

The noise-free angular velocity measurement can be written in a form similar to (10),

$$\bar{\boldsymbol{\omega}} = \tilde{\boldsymbol{\omega}} - \boldsymbol{\omega}_b - \left(\mathbf{C}_b^n \right)^T \boldsymbol{\omega}_e^n - \mathbf{n}_\omega \tag{17}$$

$$\boldsymbol{\omega}_e^n = \begin{bmatrix} \omega_e^I \cos(\theta_{lat}) & 0 & -\omega_e^I \sin(\theta_{lat}) \end{bmatrix}^T \tag{18}$$

where θ_{lat} is the degree of latitude where the navigation frame located. $\tilde{\omega}$ is the noisy angular velocity measurement. $\boldsymbol{\omega}_e^n$ is the Earth rate with respect to the navigation frame. $\mathbf{n}_\omega$ is a constant noise term. $\boldsymbol{\omega}_b$ is the rate bias which is modeled as the random walk process as well, That is,

$$\dot{\boldsymbol{\omega}}_b = \mathbf{w}_{\boldsymbol{\omega}_b} \tag{19}$$

$$\mathbf{w}_{\boldsymbol{\omega}_b} \sim \mathcal{N} \left(0, \boldsymbol{\sigma}_{\boldsymbol{\omega}_b} \right) \tag{20}$$

where $\sigma_{\boldsymbol{\omega}_b}$ is the variance of the body angular velocity. The measurement model for the GPS can be written by the following vector sum:

$$\mathbf{p}_{gps}^n = \mathbf{p}_{imu}^n + \left(\mathbf{C}_n^b \right)^T \mathbf{p}_{gps}^{imu} + \mathbf{n}_p \tag{21}$$

$$\mathbf{v}_{gps}^n = \mathbf{v}_{imu}^n + \left(\mathbf{C}_n^b \right)^T \left(\boldsymbol{\omega} \times \mathbf{r}_{gps}^{imu} \right) + \mathbf{n}_\omega \tag{22}$$

Where $\mathbf{n}_p$ and $\mathbf{n}_\omega$ are the constant noise coefficients. These formulations of the process and measurement models are discretised by time-step integrations, and are iterated in the UKF.

B. Selection of Operation Modes

The formulation of the SPKF, including the UKF which is one of its subclasses, relies on the generation of the sigma points. And these points are evaluated based on their previous state estimations and their noise covariances. Such that, for $i = 0, 1, ..., 2L$,

$$\mathcal{X}_{i,t} = \begin{cases} \hat{\mathbf{x}}_t + \sqrt{\mathbf{P}}_{i,t}, & \text{for } 0 < i \leqslant L \\ \hat{\mathbf{x}}_t - \sqrt{\mathbf{P}}_{i,t}, & \text{for } L + 1 \leqslant i \leqslant 2L \end{cases} \tag{23}$$

The matrix of sigma points,

$$\mathcal{X} = \begin{bmatrix} \hat{x}_t & \mathcal{X}_{1,t} & ... & \mathcal{X}_{2L,t} \end{bmatrix} \tag{24}$$

where L is the number of states, such that $\mathcal{X}_i \in \mathbb{R}^L$. $\hat{\mathbf{x}}$ is the estimated state vector. $\mathbf{P}_i$ is the ith column vector in the covariance matrix of the process and measurement noise terms, and the physical states. During the GNSS outage, it is obvious that the weights that reflect the degree of reliability of certain raw measurements have to be reallocated. And hence the estimation can be less susceptible to the dizzying outage readings by the GNSS. One of the direct assessments to the ambiguity of the GNSS measurements is by comparing the dilution of precisions, $\boldsymbol{\sigma}_i^{gps}$, with some pre-defined thresholds, such that,

$$\mathbf{P}_i = \begin{cases} \mathbf{P}_i^{outage}, & \text{for } norm \left(\boldsymbol{\sigma}_i^{gps} \right) \geqslant \sigma_{threshold} \\ \mathbf{P}_i^{normal}, & \text{for } norm \left(\boldsymbol{\sigma}_i^{gps} \right) < \sigma_{threshold} \end{cases} \tag{25}$$

Taking the GPS as an example, these dilutions of precisions are commonly available in the form of standard deviations and they can be extracted from the standard NMEA (National Marine Electronics Association) messages which are transmitted from the GPS devices. Although the dilution of precision is often overlooked and not used, it provides valuable information to the adjustments of the noise covariances in the UKF, so that the accuracies of the state estimations can be improved by avoiding the overvaluation on the GNSS measurements during the outage.

Original UKF Algorithm (segment)

...

4. Measurement-update equations:

4.1 $y_{k|t} = h\left(\chi_{k|t}^x, \chi_t^n\right)$

4.2 $\hat{y}_k^- = \sum_{i=0}^{2L} w_i^m y_{i,k|t}$

4.3 $P_{\hat{y}_k} = \sum_{i=0}^{2L} w_i^c \left(y_{i,k|t} - \hat{y}_k^-\right)\left(y_{i,k|t} - \hat{y}_k^-\right)^T$

4.4 $P_{x_k y_k} = \sum_{i=0}^{2L} w_i^c \left(\chi_{i,k|t}^x - \hat{x}_k^-\right)\left(y_{i,k|t} - \hat{y}_k^-\right)^T$

4.5 $K_k = P_{x_k y_k} P_{\hat{y}_k}^{-1}$

4.6 $\boxed{\hat{x}_k = \hat{x}_k^- + K_k\left(y_k - \hat{y}_k^-\right)}$

4.7 $P_{x_k} = P_{x_k}^- - K_k P_{\hat{y}_k} K_k^T$

Modified Algorithm (segment)

4.6.1 $\hat{x}_k^v = \hat{x}_k^{v-} + K_k\left(y_k - \hat{y}_k^-\right)$

4.6.2 $y_k^* = \begin{bmatrix} y_k^{pT} & \hat{x}_k^{vT} & y_k^{qT} \end{bmatrix}^T$

4.6.3 $\hat{x}_k^p = \hat{x}_k^{p-} + K_k\left(y_k^* - \hat{y}_k^-\right)$

4.6.4 $\hat{x}_k^q = \hat{x}_k^{q-} + K_k\left(y_k - \hat{y}_k^-\right)$

Fig. 9: The modified UKF algorithm. It allows the states of the position to be propagated from the latest estimations in each iteration.

TABLE I: The Performance Comparison With The Benchmark [12]

	PPS	AWNB	PPS, AWNB
Δp Improvement%	8.0593	18.4718	35.7816

	AS	PPS, AS
Δp Improvement%	13.9462	19.9808

C. Prioritised Propagation of States

In the original UKF framework, each state inherits the influences of its related ancestors from the previous iteration. It is obvious that during the GPS outage, the acceleration has to be propagated by two hierarchies of states in each iteration to fill the voids in the position and velocity measurements. The original update mechanism not only introduces latencies but also underestimations. To cope with this multiple state propagations in a single iteration, this study proposes a modification on the original UKF algorithm so that it can propagate states in time. In order to propagate the accelerations to the velocities, then to the positions in an iteration, one of the steps in the measurement-update from the original UKF algorithm is modified. The modification is shown in Fig. 9 in details. The whole idea is that the velocity estimations should have a higher priority to be updated. This modified approach first propagates the acceleration measurements to update the velocity and then the velocity estimations fill the void of the velocity measurements due to the GPS outage; and then the just-estimated velocities are propagated to update the position estimations. Finally the rest of the physical states are updated. This method avoids underestimations and the overall performance is shown in Table I.
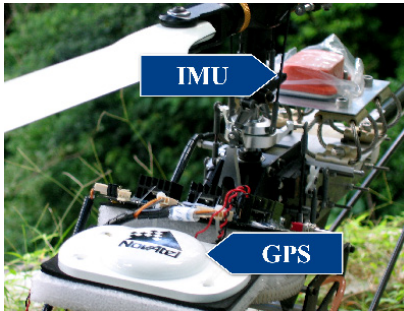

Fig. 10: The configurations of IMU and GPS antenna.

IV. Experiments

The experiments are carried out on the fully instrumented JR Voyager GSR260. Its weight is 11.2kg, length 1.48m and height 0.67m. The Xsens MTi IMU is used to measure the angular velocity, orientation and body acceleration. The geometric data are collected from the NovAtel RT2 GPS card, and the accuracy is up to ±2cm at 20Hz sampling rate as long as the satellite coverage is sufficient. The helicopter carries a mini-pc which runs with an Intel Atom 1.6GHz CPU to store all channels of data during the flight under the manual control, and are then processed in MATLAB. In addition to the implementation of our proposed method, the patented state estimation method [12] is implemented as a comparison. The results are shown in Fig. 11. It is assumed that the GPS completely malfunctions in the mid-flight (indicated as the shaded area. Each blackout lasted for fifteen seconds) and therefore switch to the GPS outage mode in the filter. As shown in Fig. 11 (a-d), our proposed method yields a referable position estimation while the previous method [12], in which our method evolved from, cannot even deliver a sensible estimation during the GPS outage (the shaded area). The poor benchmark results can be explained in twofold: (1) The benchmark method [12] consistently relied on the GPS measurement, in terms of noise covariances, for the position estimation even when the GPS experienced an outage. (2) And during the outage, the position measurement from the GPS is kept at the last known position, therefore, the benchmark estimation is kept nearly unchanged during the outage period. The proposed method deals with this method by varying its reliance to GPS measurement as well as by compensating for the disturbing noise from the IMU so that the UKF-based framework can reliably estimate the position and velocity also when the GPS measurement becomes untrustworthy. Using the proposed method, even for the minute-long GPS outages, it yields a durable and convergent estimation, and achieves a remarkable root-mean-square accuracy of ±1.98m in the position channels. The results are shown in Fig. 12.

V. Conclusion

This paper showed that it is possible to utilize simple model equations in the UKF for the localization of miniature unmanned helicopters when the GPS malfunctions completely. It is demonstrated by Monte Carlo method that the acceleration accuracy dominantly influences the position estimation errors. By analysing the Allan variances, this study proposed to model the acceleration errors not only by the random walk process, but also by the acceleration white noise bias. In order to effectively compensate for a variety of sensor errors, this study proposed a method to prioritise the propagation of states in the original UKF algorithm, and to vary the noise covariances according to the dilutions of precision. Finally, the durability and convergence of the proposed method is validated using the fully instrumented JR Voyager GSR260 helicopter. The experiments demonstrated that this approach yields a reliable position estimation while the previous work [10], in which our method evolved from, cannot even deliver a sensible estimation during the GNSS outage. The advantages of this state estimation method are that it requires neither the knowledge of the input-output kinematics on the miniature helicopter, nor that of the physical parameters like the inertia tensors. Moreover, the proposed mechanism for the noise compensation in the inertia sensors is remarkably robust against the severe vibrations due to the onboard two-stroke engine throughout the GNSS outage. The empirically proven georeferencing ability of the
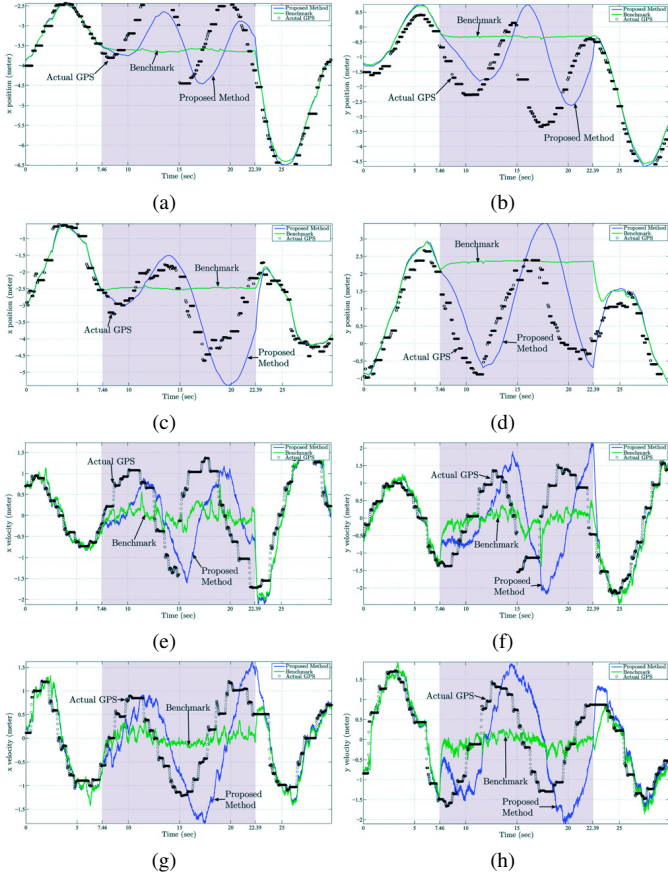
proposed method lays a foundation for unmanned helicopters to endurably react against jamming in missions.

VI. ACKNOWLEDGMENTS

Fig. 11: The performance of the proposed method and the benchmark [12] during GPS outage. The *shaded area* indicates periods of the deliberated GPS blackout, which lasted 15 seconds. (a-d) are the position estimations and (e-h) are velocity estimations. For comparison, the actual GPS measurements during the GPS outage is also plotted (in the shaded area). The deficient benchmark results are detailed in Section IV.
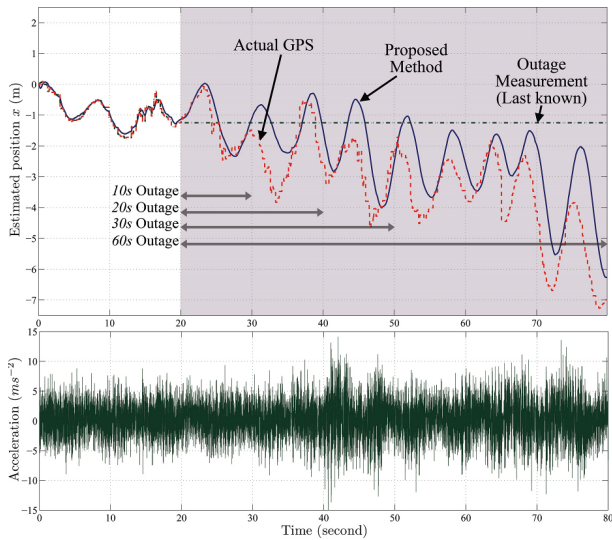

Fig. 12: The performance of the proposed method for a long period of the GPS outage. **Upper:** The *shaded area* shows the period of GPS outage. The *solid line* is the position estimation by the proposed method (AWNB and PPS). The *dash line* is the actual position measurement by the GPS for comparisons. The *dash-dot line* is the input to the state estimation method during the deliberated outage period. **Lower:** The corresponding noisy acceleration measurement in the x-axis of the body frame.

REFERENCES

[1] K. Valavanis, P. Oh, and L. Piegl, *Unmanned Aircraft Systems: International Symposium on Unmanned Aerial Vehicles, UAV'08*. Springer Verlag, 2008.

[2] P. Papadimitratos and A. Jovanovic, "Protection and Fundamental Vulnerability of GNSS," *International Workshop in Satellite and Space Communication*, October 2008.

[3] J. Carroll, "Vulnerability Assessment of the US Transportation Infrastructure that Relies on the Global Positioning System," *The Journal of Navigation*, vol. 56, no. 02, pp. 185–193, 2003.

[4] J. Anderson, "The New Wizard War: Challenges and Opportunities for Electronic Warfare in the Information Age," Joint Military Operations Department, U.S. Naval War College, Tech. Rep., 2007.

[5] O. Amidi, "An autonomous vision-guided helicopter," Ph.D. Thesis, Electrical & Computer Engg. Dept., Carnegie Mellon University, 1996.

[6] B. Steder, G. Grisetti, C. Stachniss, and W. Burgard, "Visual SLAM for Flying Vehicles," *IEEE Transactions on Robotics*, vol. 24, no. 5, pp. 1088–1093, 2008.

[7] K. Rao and M. Swamy, "New approach for suppression of FM jamming in GPS receivers," *IEEE Transactions on Aerospace and Electronic Systems*, vol. 42, no. 4, pp. 1464–1474, 2006.

[8] S. Hwang and J. Shynk, "Blind GPS receiver with a modified despreader for interference suppression," *IEEE Transactions on Aerospace and Electronic Systems*, vol. 42, no. 2, pp. 503–513, 2006.

[9] A. Abbott and W. Lillo, "Global positioning systems and inertial measuring unit ultratight coupling method," Patent, Feb 4, 2003, US Patent 6,516,021.

[10] R. van der Merwe, E. Wan, and S. Julier, "Navigation system applications of sigma-point Kalman filters for nonlinear estimation and sensor fusion," Patent, April 4, 2005, US Patent App. 11/099,433.

[11] E. Ohlmeyer, "Analysis of an ultra-tightly coupled GPS/INS system in jamming," in *2006 IEEE/ION Position, Location, And Navigation Symposium*, 2006, pp. 44–53.

[12] R. van der Merwe, E. Wan, and S. Julier, "Sigma-point Kalman filters for nonlinear estimation and sensor-fusion: Applications to integrated navigation," in *Proceedings of the AIAA Guidance, Navigation & Control Conference*, pp. 16–19.

[13] J. Wendel, O. Meister, C. Schlaile, and G. Trommer, "An integrated GPS/MEMS-IMU navigation system for an autonomous helicopter," *Aerospace Science and Technology*, vol. 10, no. 6, pp. 527–533, 2006.

[14] Z. Jiang, Q. Song, Y. He, and J. Han, "A novel adaptive unscented Kalman filter for nonlinear estimation," in *Decision and Control, 2007 46th IEEE Conference on*, 2007, pp. 4293–4298.

[15] S. Tompkins, "Robust Surface Navigation (RSN)." http://www.darpa.mil/STO/space/rsn.html.

[16] D. Biezad, *Integrated navigation and guidance systems*. Reston, VA: AIAA, 1999.

[17] R. Hayward, D. Gebre-Egziabher, M. Schwall, J. Powell, and J. Wilson, "Inertially Aided GPS Based Attitude Heading Reference System (AHRS) for General Aviation Aircraft," in *Proceedings of the Institute of Navigation ION-GPS Conference*, 1997, pp. 1415–1424.

[18] P. Savage, "Strapdown inertial navigation integration algorithm design part 2: Velocity and position algorithms," *Journal of Guidance Control and Dynamics*, vol. 21, pp. 208–221, 1998.

[19] ——, "Strapdown inertial navigation integration algorithm design part 1: Attitude algorithms," *Journal of Guidance Control and Dynamics*, vol. 21, pp. 19–28, 1998.

[20] D. Titterton and J. Weston, *Strapdown inertial navigation technology*. Peter Peregrinus Ltd., London, 2004.

[21] J. Stambaugh and S. Falls, "Propagation and system accuracy impact of major sensor errors on a strapdown aircraft navigator," *IEEE Transactions on Aerospace and Electronic Systems*, 1973.

[22] A. Saltelli, M. Ratto, T. Andres, F. Campolongo, J. Cariboni, D. Gatelli, M. Saisana, and S. Tarantola, *Global sensitivity analysis: the primer*. Wiley-Interscience, 2008.

[23] N. El-Sheimy, H. Hou, and X. Niu, "Analysis and modeling of inertial sensors using allan variance," *IEEE Transactions on Instrumentation and Measurement*, vol. 57, no. 1, pp. 140–149, 2008.

[24] D. Allan, H. Hellwig, P. Kartaschoff, J. Vanier, J. Vig, G. Winkler, N. Yannoni, and B. NBS, "Standard terminology for fundamental frequency and time metrology," in *Frequency Control Symposium, 1988., Proceedings of the 42nd Annual*, 1988, pp. 419–425.

[25] IEEE Std. 952-1997, *IEEE Standard Specification Format Guide and Test Procedure for Single-Axis Interferometric Fiber Optic Gyros*. Piscataway, NJ, USA: IEEE Standards, 1998.

[26] A. Doucet, N. De Freitas, and N. Gordon, *Sequential Monte Carlo methods in practice*. Springer Verlag, 2001.

[27] S. Julier and J. Uhlmann, "A new extension of the Kalman filter to nonlinear systems," in *Int. Symp. Aerospace/Defense Sensing, Simul. and Controls*, vol. 3, 1997, p. 26.

[28] B. Stevens and F. Lewis, *Aircraft Control and Simulation*. John Wiley and Sons, Inc., NY, 1992.